Front. Optoelectron. 2014, 7(1): 37–45
DOI 10.1007/s12200-014-0389-3

RESEARCH ARTICLE

Hydrazine processed Cu_2SnS_3 thin film and their application for photovoltaic devices

Jun HAN[1], Ying ZHOU[2], Yang Tian[3], Ziheng HUANG[4], Xiaohua WANG (✉)[1], Jie ZHONG[2], Zhe XIA[2], Bo YANG[2], Haisheng SONG[2], Jiang TANG (✉)[2]

1 School of Science, Changchun University of Science and Technology, Changchun 130022, China
2 Wuhan National Laboratory for Optoelectronics (WNLO), Huazhong University of Science and Technology, Wuhan 430074, China
3 Department of Environmental Science, College of Environmental Sciences, Minzu University of China, Beijing 100081, China
4 School of Optical and Electronic Information, Huazhong University of Science and Technology, Wuhan 430074, China

Abstract Copper tin sulfide (Cu_2SnS_3) was a potential earth abundant absorber material for photovoltaic device application. In this contribution, triclinic Cu_2SnS_3 film with phase pure composition and large grain size was fabricated from a hydrazine solution process using Cu, Sn and S as the precursors. Absorption measurement revealed this Cu_2SnS_3 film had a direct optical band gap of 0.88 eV, and Hall effect measurement indicated the film was p-type with hole mobility of 0.86 cm^2/Vs. Finally Mo/Cu_2SnS_3/CdS/ZnO/AZO/Au was produced and the best device efficiency achieved was 0.78%. Also, this device showed improved device performance during ambient storage. This study laid some foundation for the further improvement of Cu_2SnS_3 solar cell.

Keywords copper tin sulfide (Cu_2SnS_3), solar cell, hydrazine, solution process, triclinic

1 Introduction

Copper tin sulfide (Cu_2SnS_3) is a promising absorber material for thin film photovoltaic due to its suitable optoelectronic properties and attractive raw-material features. Depending on its crystal structure, Cu_2SnS_3 has direct band gaps ranging from 0.93–1.51 eV covering the visible and near-infrared part of solar spectrum [1,2]. It also has large absorption coefficient exceeding 10^4 cm^{-1} at energies right above the band gap, and possesses naturally p-type doping with hole mobility of 80 cm^2/Vs [3]. On materials side, Cu_2SnS_3 is a compound composed of non-toxic, inexpensive and earth-abundant elements. Its ternary nature also contains less types of crystal defects as compared to copper zinc tin sulfoselenide (CZTSSe), reducing the complexicity of phase and defect control in CZTS system [4,5]. Consequently, thin film solar cells using Cu_2SnS_3 as the absorber received increased research interest in these years [3,6,7]. For example, Berg et al. produced monoclinic Cu_2SnS_3 film by annealing electrodeposited precursor in a sulfur and tin sulfide environment and achieved photovoltaic device efficiency of 0.54% [8]. In 2012, Koike et al. optimized the composition of electrodeposited Cu_2SnS_3 film and produced an impressive device efficiency of 2.84%, the highest efficiency for Cu_2SnS_3 solar cell reported so far [9].

In this paper, we presented the fabrication of Cu_2SnS_3 film using a hydrazine process. Hydrazine has strong capability to dissolve metal chalcogenide in the presence of excess chalcogens without introducing carbon and oxygen impurities and could result in device quality chalcogenide films after thermal annealing [10]. Consequently, high quality metal chalcogenide field effect transistors [11] and world record efficiency CZTSSe solar cells [12,13] were produced using hydrazine process. We thus adopted this strategy to produce high quality Cu_2SnS_3 film for material characterization and photovoltaic device application. Cu, Sn and S elements were directly dissolved into hydrazine to prepare the solution for spin-coating. The spin-coated film was then annealed inside a N_2 filled glovebox to generate Cu_2SnS_3 film with phase-pure composition and large grain size. As produced Cu_2SnS_3 film was characterized as triclinic with an optical band gap of 0.88 eV, having p-type doping with hole mobility of 0.86 cm^2/Vs. We further integrated our Cu_2SnS_3 film into a heterojunction solar cell achieving

Received November 13, 2013; accepted December 3, 2013

E-mail: jtang@mail.hust.edu.cn, biewang2001@126.com

solar conversion efficiency of 0.78%.This study laid the foundation for the further advancement of earth abundant, low-cost Cu_2SnS_3 solar cells.

2 Experiments

2.1 Fabrication of Cu_2SnS_3 thin film

Cu_2SnS_3 thin film was fabricated from a layer-by-layer spin-coating method using hydrazine solution. First, 0.315 g Cu power and 0.238 g S flakes were weighted and then 3 mL hydrazine (containing 2% water) was quickly injected. Similarly, 0.356 g Sn powder and 0.384 g S flakes were weighted and then 3 mL hydrazine was quickly injected. After stirring for 2 days, a clear red (Cu-S) or light-green (Sn-S) hydrazine solution was obtained. These two solutions were mixed together with the addition of 10 μL Sb_2S_3 hydrazine stock solution and 25 μL Na_2S hydrazine stock solution to prepare the precursor solution ready for spin-coating. *Caution: Hydrazine is highly flammable and toxic; all operation should be done inside a glovebox with great care!*

Molybdenum covered soda lime glass was carefully rinsed with ammonium solution (28% – 30% concentration) and then used as the substrate for film deposition. A few drops of Cu_2SnS_3 precursor solution was spread onto the substrate, then spun (400 r/min, 4 s; 800 r/min, 20 s; 2100 r/min, 20 s) and baked at 80°C on a hotplate for 5 min to evaporate hydrazine. The film was further baked at 425°C for 2 min to remove excess S contained inside the film. This spin-dry-bake process was repeated for another 4 times to yield the film with desired thickness. Finally the film was baked at 600°C on a hotplate with the addition of excess sulfur for 20 min and then naturally cooled down on asbestos substrates. Extreme carefulness should be applied during the operation to minimize sudden temperature change and avoid glass breakage.

2.2 Heterojunction solar cell preparation

Heterojunction solar cell Mo/Cu_2SnS_3/CdS/i-ZnO/Al-ZnO/Au was fabricated as follows: first Cu_2SnS_3 film was prepared on Mo substrates according to the procedure described above. Then CdS buffer layer was deposited using the standard chemical bath deposition ($CdSO_4$, thiourea, $NH_3 \cdot H_2O$ react at 65°C for 13 min) [14]; ZnO and Al doped zinc oxide (AZO) were subsequently sputtered onto the devices kept at 200°C. Sputtering condition for ZnO was 0.2 Pa Ar pressure, 100 W power for 8 min; for AZO was 0.2 Pa Ar pressure, 300 W power for 40 min. Finally Au electrodes were e-beam evaporated to complete the device. No antireflection layer was deposited, and the device was mechanically scribed to define the device area.

2.3 Materials and device characterization

Cu_2SnS_3 thin film and photovoltaic device were carefully characterized. Cu_2SnS_3 precursor solution was naturally dried inside glovebox to yield a gel for thermo gravimetric analysis (TGA). TGA was done on Perkin Elmer Instruments (Diamond TG/DTA6300) with a heating rate of 10°C/min under N_2 flow. Power X-ray diffraction (Philips, X pert pro MRD), scanning electron microscopy (SEM, FEI Nova NanoSEM450, without Pt coating) and X-ray photoelectron spectroscopy (XPS, EDAX Inc. Genesis) measurements were done directly using the Cu_2SnS_3 film. For XPS measurement, C 1s peak at 284.8 eV was applied for calibration. Film transmittance was carried out on Cu_2SnS_3 film deposited onto fluorine-doped tin oxide (FTO) using Perkin Elmer Instruments (Lambda950) with an integrating sphere. For solar cell measurement, the device was mechanically scribed into 0.40 cm^2 area. A solar simulator with a Xe light source (450 W, Oriel, model 9119) and an AM1.5G filter was used to produce the simulated 100 mW/cm^2 solar irradiation. Current density-voltage characteristics were measured using a Keithley 2400 source-meter in the air. No intentional temperature control or aperture was used for the efficiency measurement.

3 Results and discussion

3.1 Film fabrication and optimization

Hydrazine process was applied to fabricate Cu_2SnS_3 thin film. First, Cu and excess S (molar ratio Cu:S = 1.0:1.5), and Sn and excess S (molar ratio Sn:S = 1.0:4.0) were mixed and stirred for days to yield a clear solution. For conventional hydrazine process, Cu_2S and SnS_2 were used as the Cu and Sn precursors [13,15]. We preferred metal precursor over metal sulfide because commercial Cu_2S and SnS_2 raw materials often deviate from perfect stoichiometry and contain impurities such as $Cu_{2-x}S$ and SnS_{2-x}. The batch to batch variation often jeopardizes precise composition control and device reproducibility. In practice, we adjusted the amount of sulfur added and the speed of hydrazine injection to get fully dissolved Cu and Sn solution. No difference in terms of solution appearance and film morphology was observed when use metal instead of metal sulfide as the precursors. Metal power and S flakes might react in situ and experience different reaction pathways as compared to reaction using metal sulfide precursors, but they probably evolved into the same final products when fully dissolved into hydrazine. Figure 1(a) presents digital images of Cu-S and Sn-S hydrazine solution and the mixed Cu-Sn-S precursor solution. Both Cu-S and Sn-S solution were clear without any detectable precipitates; when mixed together, the solution remained

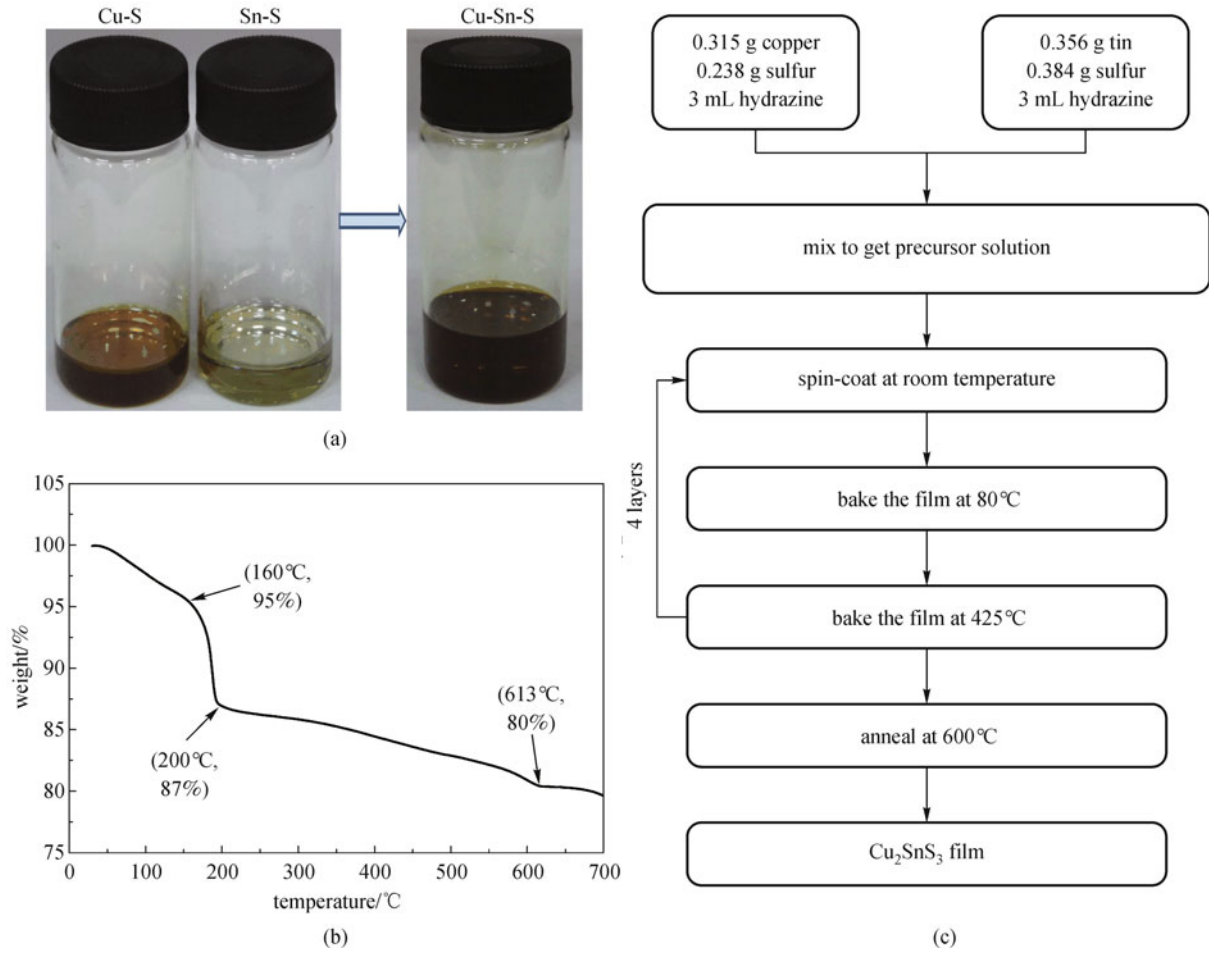

Fig. 1 Cu_2SnS_3 solution preparation and film fabrication. (a) Digital images of Cu-S, Sn-S and Cu-Sn-S hydrazine solution; (b) TGA curve of Cu-Sn-S precursor powder (dried inside glovebox) measured in N_2 atmosphere; (c) flowing chart of Cu_2SnS_3 film fabrication procedure

clear, suggesting the molecular level dissolution of Cu and Sn into hydrazine [10]. Trace amount of Na and Sb dopants were introduced during the mixing to promote Cu_2SnS_3 defects passivation and grain growth, respectively, similar to the copper indium gallium selenide (CIGS) [16,17] and CZTSSe [12] case.

TGA of the dried Cu-Sn-S precursor solution was carried out to investigate the temperature dependent hydrazine and excess sulfur loss (Fig. 1(b)). Since the boiling temperature of hydrazine and melting point of sulfur are 114°C and 115°C, respectively, we attributed the first 5% weight loss (room temperature to 160°C) to the leaving of freely presented hydrazine and sulfur and the second abrupt 8% weight loss (160°C–200°C) to decomposition of solute species such as $N_4H_9Cu_7S_4$ and $(N_2H_5)_4Sn_2S_6$. As proposed by Mitzi, the decomposition products for $N_4H_9Cu_7S_4$ and $(N_2H_5)_4Sn_2S_6$ were N_2H_4 and H_2S, Cu_2S and SnS_2 respectively [10]. The evaporation of Cu_2S and more likely SnS_2, a compound known for its high vapor pressure [18], accounted for a further gradual 7% weight loss up to 600°C. At temperature higher than 600°C, no further weight loss was observed which indicated that Cu_2SnS_3 formation was completed.

Since a total of 20% weight loss was accompanied during the whole heating process, layer-by-layer spin-coating was applied to fabricate Cu_2SnS_3 film because the cracks and pinholes associated with significant weight loss in the underlying layer could be filled by the subsequent layer on top [19]. In addition, the number of deposited layers controlled film thickness. Guided by this principle and the data from TGA measurement, we spun our Cu-Sn-S precursor solution and then applied a pre-bake step at 80°C to eliminate hydrazine, a soft-bake step at 425°C to remove excess sulfur and decompose the precursors. This process was repeated for another 4 times to yield a film with desired thickness. Finally the film was subjected to a hard-bake at 600°C to complete Cu_2SnS_3 formation and grain growth. The film fabrication procedure was shown as a flowing chart in Fig. 1(c), and the key optimization steps would be discussed later.

To achieve Cu_2SnS_3 film with good film morphology, the conditions for the hard-bake was crucial. For solar cell

application, compact film without any cracks and pinholes is a must to avoid shunting problems, and large grain size is preferred to minimize recombination at grain boundaries and promote carrier transport within the grain [20]. Annealing temperature and environment are key parameters to achieve optimal film morphology. We first studied the hard-bake temperature. For these experiments, films were subjected to the same pre-bake and soft-bake steps, and 5 mg sulfur was added to the annealing environment, the only difference being the hard-bake temperature. Four temperatures were investigated: 450°C, 500°C, 550°C and 600°C. As shown in Fig. 2, top-view SEM characterization revealed that when hard-baked at temperature below 600°C, the film was porous containing many cracks and pores. Also, the grain size increased as the annealing temperature increased. When hard-baked at 600°C, the film was crack- and pinhole-free and the grains reached micrometer size. Higher temperature resulted in faster ions' thermal movement, promoting diffusion and consequently promoting grain growth and sintering.

We further investigated the amount of sulfur addition during hard-bake at 600°C. Figure 3 shows the top-view and cross-sectional SEM images of Cu_2SnS_3 film baked at 600°C with the addition of 0, 1 and 10 mg sulfur powder. The amount of sulfur addition, or equivalently the sulfur vapor pressure, had little influence on the film thickness because for all three samples, Cu_2SnS_3 film was 1.0 – 1.3 μm thick. However, sulfur addition played a paramount effect on film morphology. When no sulfur presented, film was compact and the grain size was large. Unfortunately, there was a thin fluffy layer on top, in addition to some scattered points which were believed to be secondary phases. Energy dispersive X-ray analysis of Cu_2SnS_3 film surface observed more sulfur than its stoichiometric value. When 10 mg sulfur was introduced, the film was very porous containing many pores, and the grain size was not satisfactory. When 1 mg sulfur was presented, the film was crack-, pinhole- and secondary phase-free from the top view SEM observation, and the grains were large and compact from cross-sectional SEM observation. Such a high quality Cu_2SnS_3 is comparable to the state-of-the-art CZTS film [12] and paves its way for film characterization and device application. Sulfur pressure governed the delicate equilibrium between possible Cu_2SnS_3 decomposition, SnS and SnS_2 evaporation, and grain sintering and growth, probably in a similar fashion as in the CZTS system [18]. The detailed underlying mechanism is a subject for further investigation.

3.2 Film characterization

We applied X-ray diffraction (XRD), Raman spectroscopy and absorption measurement to study the phase and optical properties of as-obtained film. Figure 4(a) presents the XRD patterns of our film. The position and relative intensities of diffraction peaks agreed very well with the standard triclinic Cu_2SnS_3 (JCPDS 027-0198). The standard patterns and the indices of major diffraction peaks were included for comparison and clarity. Apart from the Mo substrate, no secondary phase such as SnS and Cu_2S was observed within XRD detection. Depend on

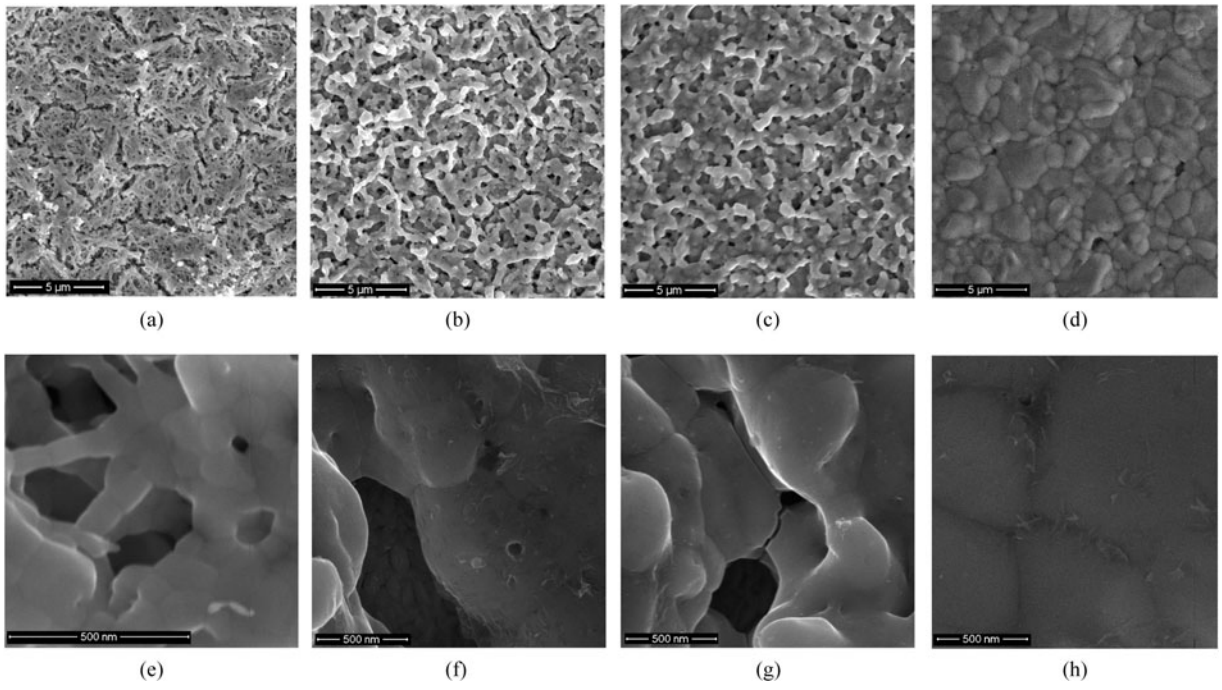

Fig. 2 Top-view SEM images of Cu_2SnS_3 film annealed at different temperatures for 10 min. (a) and (e) 450°C; (b) and (f) 500°C; (c) and (g) 550°C; (d) and (h) 600°C. Sulfur addition was kept as 5 mg for all samples

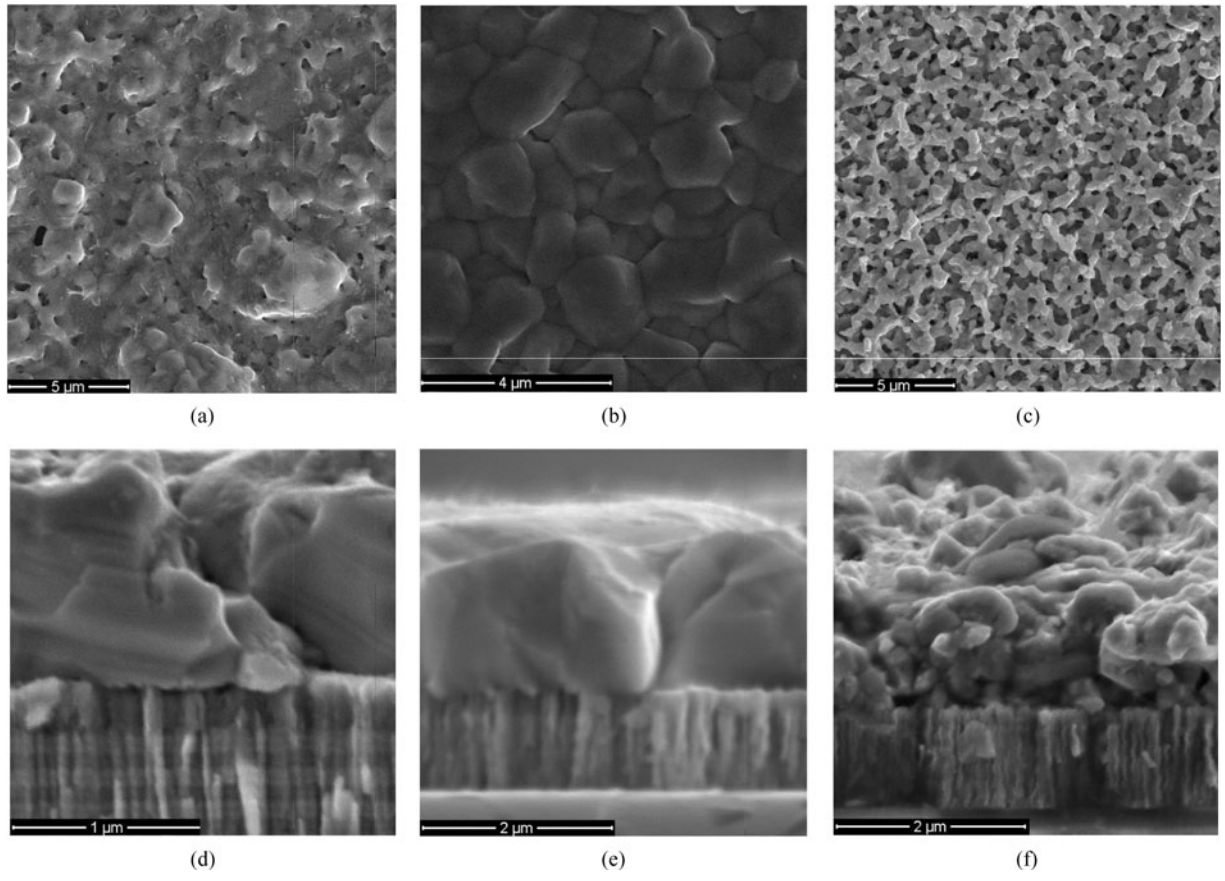

Fig. 3 Top-view and cross-sectional SEM images of Cu_2SnS_3 film annealed at 600 °C with different amount of sulfur addition. (a) and (d) 0 mg; (b) and (e) 1 mg; (c) and (f) 10 mg

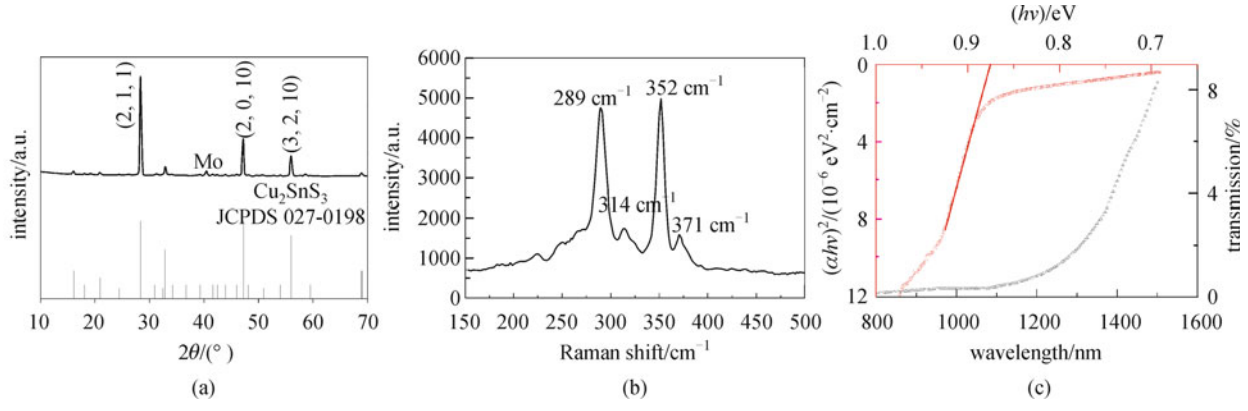

Fig. 4 Characterization of Cu_2SnS_3 film. (a) XRD pattern of Cu_2SnS_3 film on Mo substrate. The major diffraction peaks of (2,1,1), (2,0,10) and (3,2,10) and the standard triclinic Cu_2SnS_3 diffraction peaks (JCPDS 027-0198) were included; (b) Raman spectrum of Cu_2SnS_3 film with the position of 4 peaks included; (c) absorption spectrum and corresponding $(\alpha h\nu)^2$ vs. $(h\nu)$ fitting to extract the optical band gap of Cu_2SnS_3 film

the local cation coordination around anions, Cu_2SnS_3 has cubic, monoclinic and triclinic phases and monoclinic and triclinic are phases stabilized at low temperatures (< 775°C) [21]. Literature reported that different film fabrication procedure and heat treatment history results in Cu_2SnS_3 film with different phases like tetragonal or monoclinic or cubic [22,23].Our hydrazine process probably favored cation distributions as in triclinic phase.

Raman spectrum is a standard tool to analyze the composition and phase of target substance. We applied Raman analysis to check our Cu_2SnS_3 film. Two dominant Raman peaks centered at 289 and 352 cm^{-1}, characteristic

of a′vibration symmetry of Cu_2SnS_3, was observed in Fig. 4(b). The two additional peaks with reduced intensities at 314 and 371 cm^{-1} were also originated from Cu_2SnS_3 phase, in concordance with previous literature report [21]. In a word, both XRD and Raman results confirmed our film was pure Cu_2SnS_3.

The value of band gap is crucial for a potential photovoltaic absorber material. Absorption measurement was applied to measure the absorption onset of Cu_2SnS_3 film. As shown in Fig. 4(c), Cu_2SnS_3 showed a strong absorption starting from ~1200 nm (black line). By plotting $(\alpha hv)^{0.5}$ vs. (hv) and fitting the linear part, we obtained the intersect with x-axis as 0.88 V, the direct band gap of Cu_2SnS_3. We could not get a nice linear zone when plot $(\alpha hv)^2$ vs. (hv), thus ruling out the possibility of Cu_2SnS_3 being an indirect band gap material. This measured value supported previous theoretical simulation of Cu_2SnS_3 where a direct band gap of 0.8–0.9 eV was predicted [1]. This value, however, it is relatively small and deviated from the optimal value, 1.0–1.5 eV for thin film solar cells, suggesting that alloying with oxygen or germanium [24] to increase its band gap might be needed for high efficiency Cu_2SnS_3 based photovoltaic devices.

XPS was employed to investigate the film's chemistry nature. Figure 5 presents the XPS spectra of Cu, Sn and S elements of fresh Cu_2SnS_3 sample. The binding energy of Cu $2p^{1/2}$ and $2p^{3/2}$ was 952.5 and 932.8 eV, respectively. Both peaks were characteristic of Cu^+ [25]. Similarly, the binding energy of Sn $3d^{3/2}$ and $3d^{5/2}$, S $2p^{1/2}$ and $2p^{3/2}$ was 495.2 and 486.7 eV, 163.1 and 162.0 eV, in good agreement with Sn^{4+} and S^{2-}, respectively. The perfect Gaussian-Lorentzian peak fitting for all these three peaks excluded the presence of Cu^{2+}, Sn^{2+} and S in the sample within XPS detection limit. The right stoichiometry in combination with the desired element valences further confirmed our film was Cu_2SnS_3.

Hall effect measurement was further employed to study the electrical properties of our Cu_2SnS_3 film. Samples were prepared by depositing Cu_2SnS_3 film on insulating substrates with four Au electrodes at the corner as contacts. The measured Hall coefficient R_H was 1.30 cm^3/C confirming our Cu_2SnS_3film was p-type. Based on the equation that $R_H = 1/(pq)$, where p is hole concentration and q is elemental charge, we estimated hole concentration as 4.8×10^{18} cm^{-3}. The measured film conductivity was 0.66 $\Omega^{-1}\cdot cm^{-1}$ and hole mobility was estimated to be 0.86 cm^2/Vs. These values were similar to Cu_2SnS_3 film derived from direct liquid coating, where hole concentration of 3.71×10^{18} cm^{-1} and mobility of 0.93 cm^2/Vs was obtained [6].

3.3 Device performance and stability

Last we checked the photovoltaic device performance using Cu_2SnS_3 as the absorber. Device configuration is schematically shown in Fig. 6(a). Mo coated soda lime glass was used as the substrates and back contact; CdS derived from chemical bath deposition was applied as the buffer layer to form the heterojunction with Cu_2SnS_3 absorber; ZnO was sputtered to increase device shunt resistance; AZO was also sputtered on top to serve as the transparent conductive oxide (TCO), and Au electrodes were e-beam evaporated to work as the top electrodes. Light was shed from the AZO side, passing from the AZO, ZnO and CdS layer and being absorbed by the Cu_2SnS_3 layer. Photogenerated carriers were separated at the Cu_2SnS_3/CdS interface; electrons injected into CdS layer and finally collected by the top Au electrodes, and holes travelled through the Cu_2SnS_3 layer and were finally collected by the bottom Mo electrodes.

The typical current density-voltage (J-V) curves of our Cu_2SnS_3 solar cells in the dark and fewer than 100 mW/cm^2 simulated AM1.5G illumination were presented in Fig. 6(b). This device showed pretty poor rectification in the dark, suggesting the quality of Cu_2SnS_3/CdS heterojunction interface needs further improvement. Under light irradiation, the best device demonstrated an open circuit voltage (V_{oc}) of 0.199 V, a short circuit current density (J_{sc}) of 14.2 mA/cm^2, and a fill factor (FF) of 27.4%, corresponding to an energy conversation efficiency of 0.78%. Aside from this champion device, multiple devices with efficiency exceeding 0.6% have been successfully fabricated. The champion device showed a small shunt resistance of only 45.4 Ω and a large series resistance of

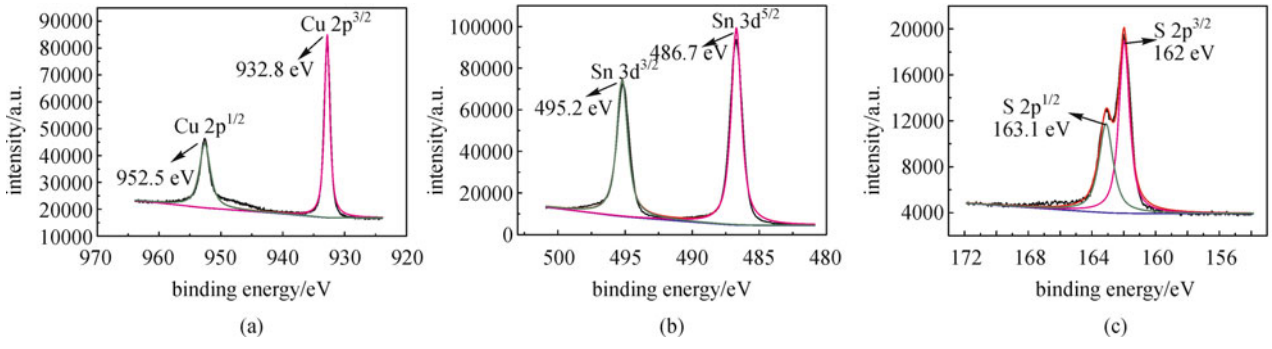

Fig. 5 XPS spectra of Cu, Sn and S element in Cu_2SnS_3 film. (a) Cu; (b) Sn; (c) S. Black curves were original data and pink and green curves were Gaussian-Lorentzian fitting curves

29.4 Ω, giving rise to the low *FF*. Our device characteristics echoed previous Cu_2SnS_3 solar cells where large J_{sc} yet low V_{oc} were generally reported [8,9,23]. For example, Chino et al. presented Cu_2SnS_3 solar cell with champion device [23] showing V_{oc} of 0.211 V and J_{sc} of 28 mA/cm^2. Such a low V_{oc} severely limited overall device performance. The underlying reason was unclear at present, and solving the low V_{oc} associated with Cu_2SnS_3 photovoltaic devices should be the major thrust for the future research.

Finally, we checked the storage stability of our Cu_2SnS_3 device. Three representative devices A, B, and C were stored in ambient laboratory environment and their device performance was periodically measured. For all three checked devices, device efficiencies monotonically increased during ambient storage (Fig. 6(c)). The largest efficiency augment was observed in device A where the initial device efficiency was 0.35% and after 80 days ambient storage, device efficiency soared up to 0.72%. We compared in detail the device characteristics of solar cell B (shown in Fig. 6(d)): fresh device showed a V_{oc} of 0.218 V, J_{sc} of 9.6 mA/cm^2 and *FF* of 25.3%, corresponding to an efficiency of 0.53%; after 80 days laboratory storage the aged device showed a V_{oc} of 0.229 V, J_{sc} of 12.1 mA/cm^2 and *FF* of 25.5%, corresponding to an efficiency of 0.70%. Device efficiency improvement during ambient storage was also encountered in CIGS and CZTS solar cells, and this might be resulted from the improved interface quality such as the Cu_2SnS_3/CdS junction interface or the CdS/ZnO interface during storage. Mechanism study will be done to uncover the reason behind.

4 Conclusions

In summary, we demonstrated fabrication of high quality Cu_2SnS_3 film from hydrazine process using Cu, Sn and S element as the precursors. By optimizing the amount of sulfur addition and annealing temperature, triclinic Cu_2SnS_3 film with high crystallinity and large grain size

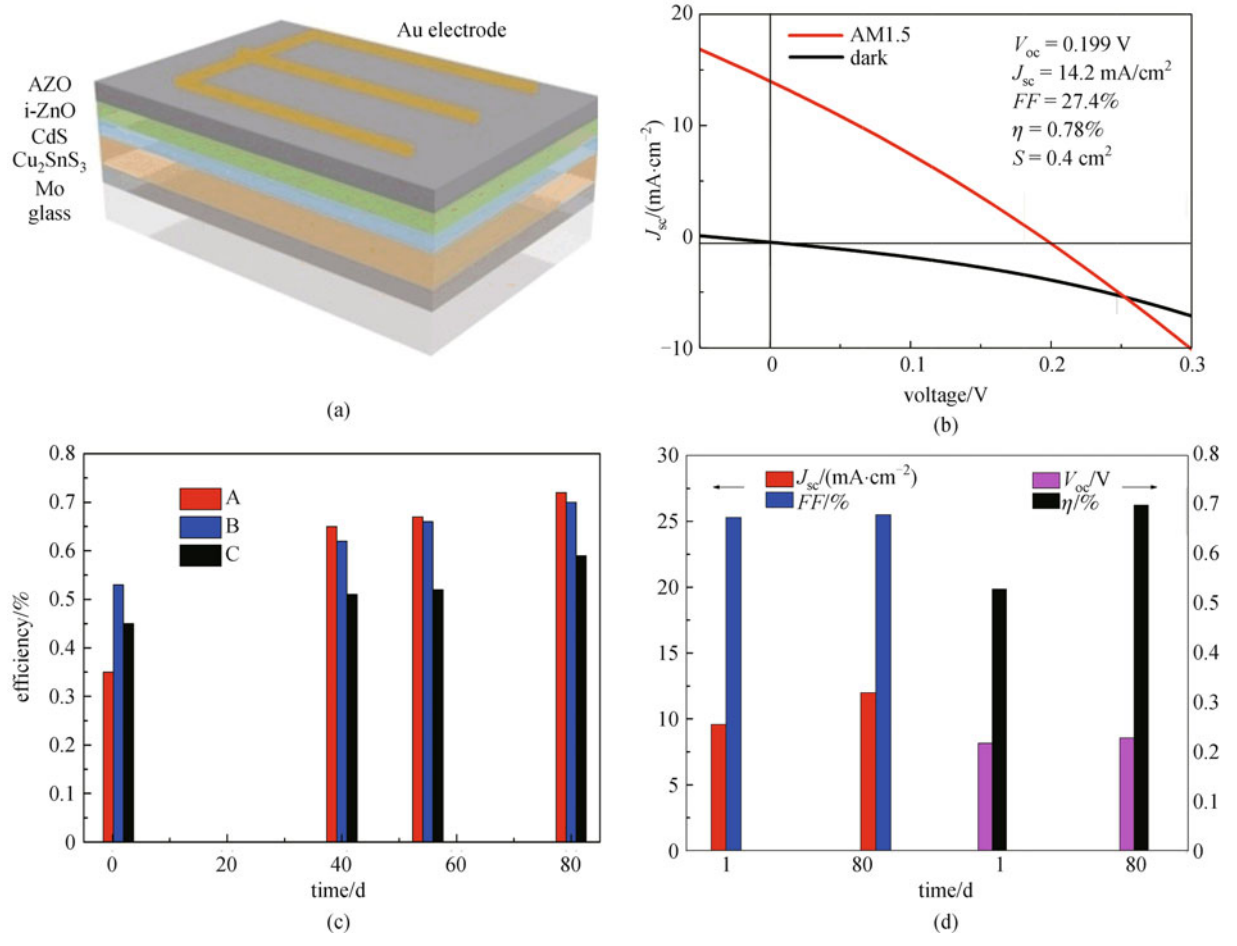

Fig. 6 Solar cell configuration, performance and stability. (a) Schematic demonstration of the device configuration of Cu_2SnS_3 solar cell; (b) dark and light *J-V* curves of Cu_2SnS_3 solar cell. Light was simulated AM1.5G irradiation at an intensity of 100 mW/cm^2; (c) efficiency evolution of three representative unencapsulated devices A, B, C when stored in lab environment for 0, 40, 55 and 80 days; (d) comparison of device characteristics V_{oc}, J_{sc}, *FF* and η between fresh (0 day storage) and aged (80 days ambient storage) of Cu_2SnS_3 photovoltaic device B

was obtained. The film had a direct band gap of 0.88 eV estimated from optical absorption measurement, and hall measurement showed the film was p-type with hole mobility of 0.86 cm^2/Vs. Finally, Cu_2SnS_3/CdS heterojunction solar cells were constructed and achieved a solar conversion efficiency of 0.78%. Further research should focus on the increase of band gap through alloying and consequently V_{oc} improvement to guarantee its promising application for photovoltaic devices.

Acknowledgements This work was financially supported by the National Natural Science Foundation of China (Grant Nos. 61274055, 61322401, 61006065, 61076039 and 61204065), National 1000 Young Talents Project and the Fundamental Research Funds for the Central Universities (HUST: 0118187043). The authors thank the Analytical and Testing Center of Huazhong University of Sciences and Technology (HUST) and the Center of Micro-Fabrication and Characterization (CMFC) of Wuhan National Laboratory for Optoelectronics (WNLO) for facility access. We would also like to acknowledge Innovative Technology and Beijing Technol Science Co. Ltd for glovebox and thermal evaporator technical assistance, respectively.

References

1. Zhai Y T, Chen S, Yang J H, Xiang H J, Gong X G, Walsh A, Kang J, Wei S H. Structural diversity and electronic properties of Cu_2SnX_3 (X = S, Se): a first-principles investigation. Physical Review B: Condensed Matter and Materials Physics, 2011, 84(7): 075213–075216
2. Bouaziz M, Ouerfelli J, Srivastava S K, Bernede J C, Amlouk M. Growth of Cu_2SnS_3 thin films by solid reaction under sulphur atmosphere. Vacuum, 2011, 85(8): 783–786
3. Avellaneda D, Nair M T S, Nair P K. Cu_2SnS_3 and Cu_4SnS_4 thin films via chemical deposition for photovoltaic application. Journal of the Electrochemical Society, 2010, 157(6): D346–D352
4. Chen S Y, Walsh A, Gong X G, Wei S H. Classification of lattice defects in the kesterite Cu_2ZnSnS_4 and $Cu_2ZnSnSe_4$ earth-abundant solar cell absorbers. Advanced Materials, 2013, 25(11): 1522–1539
5. Chen S Y, Wang L W, Walsh A, Gong X G, Wei S H. Abundance of CuZn + SnZn and 2CuZn + SnZn defect clusters in kesterite solar cells. Applied Physics Letters, 2012, 101(22): 223901–223904
6. Tiwari D, Chaudhuri T K, Shripathi T, Deshpande U, Rawat R. Non-toxic, earth-abundant 2% efficient Cu_2SnS_3 solar cell based on tetragonal films direct-coated from single metal-organic precursor solution. Solar Energy Materials and Solar Cells, 2013, 113: 165–170
7. Chen Q M, Dou X M, Ni Y, Cheng S Y, Zhuang S L. Study and enhance the photovoltaic properties of narrow-bandgap Cu_2SnS_3 solar cell by p-n junction interface modification. Journal of Colloid and Interface Science, 2012, 376(1): 327–330
8. Berg D M, Djemour R, Gutay L, Zoppi G, Siebentritt S, Dale P J. Thin film solar cells based on the ternary compound Cu_2SnS_3. Thin Solid Films, 2012, 520(19): 6291–6294
9. Koike J, Chino K, Aihara N, Araki H, Nakamura R, Jimbo K, Katagiri H. Cu_2SnS_3 thin-film solar cells from electroplated precursors. Japanese Journal of Applied Physics, 2012, 51(10): 10NC34-1–10NC34-3
10. Mitzi D B. Solution processing of chalcogenide semiconductors via dimensional reduction. Advanced Materials, 2009, 21(31): 3141–3158
11. Mitzi D B, Kosbar L L, Murray C E, Copel M, Afzali A. High-mobility ultrathin semiconducting films prepared by spin coating. Nature, 2004, 428(6980): 299–303
12. Todorov T K, Tang J, Bag S, Gunawan O, Gokmen T, Zhu Y, Mitzi D B. Beyond 11% efficiency: characteristics of state-of-the-art $Cu_2ZnSn(S,Se)_4$ solar cells. Advanced Energy Materials., 2013, 3 (1): 34–38
13. Todorov T K, Reuter K B, Mitzi D B. High-efficiency solar cell with Earth-abundant liquid-processed absorber. Advanced Materials, 2010, 22(20): E156–E159
14. Contreras M A, Romero M J, To B, Hasoon F, Noufi R, Ward S, Ramanathan K. Optimization of CBD CdS process in high-efficiency $Cu(In,Ga)Se_2$-based solar cells. Thin Solid Films, 2002, 403–404: 204–211
15. Yang W B, Duan H S, Bob B, Zhou H P, Lei B, Chung C H, Li S H, Hou W W, Yang Y. Novel solution processing of high-efficiency Earth-abundant $Cu_2ZnSn(S,Se)_4$ solar cells. Advanced Materials, 2012, 24(47): 6323–6329
16. Yuan M, Mitzi D B, Liu W, Kellock A J, Chey S J, Deline V R. Optimization of CIGS-based PV dedvice through antimony doping. Chemistry of Materials, 2010, 22(2): 285–287
17. Cao Q, Gunawan O, Copel M, Reuter K B, Chey S J, Deline V R, Mitzi D B. Defects in $Cu(In,Ga)Se_2$ chalcopyrite semiconductors: a comparative study of material properties, defect states, and photovoltaic performance. Advanced Energy Materials, 2011, 1 (5): 845–853
18. Redinger A, Berg D M, Dale P J, Siebentritt S. The consequences of kesterite equilibria for efficient solar cells. Journal of the American Chemical Society, 2011, 133(10): 3320–3323
19. Tang J, Brzozowski L, Barkhouse D A R, Wang X H, Debnath R, Wolowiec R, Palmiano E, Levina L, Pattantyus-Abraham A G, Jamakosmanovic D, Sargent E H. Quantum dot photovoltaics in the extreme quantum confinement regime: the surface-chemical origins of exceptional air- and light-stability. ACS Nano, 2010, 4(2): 869–878
20. Tian Q W, Xu X F, Han L B, Tang M H, Zou R J, Chen Z G, Yu M H, Yang J M, Hu J Q. Hydrophilic Cu_2ZnSnS_4 nanocrystals for printing flexible, low-cost and environmentally friendly solar cells. CrystEngComm, 2012, 14(11): 3847–3850
21. Berg D M, Djemour R, Gütay L, Siebentritt S, Dale P J, Fontane X, Izquierdo-Roca V, Pérez-Rodriguez A. Raman analysis of monoclinic Cu_2SnS_3 thin films. Applied Physics Letters, 2012, 100(19): 192103–192104
22. Fernandes P A, Salomé P M P, Cunha A F. A study of ternary Cu_2SnS_3 and Cu_3SnS_4 thin films prepared by sulfurizing stacked metal precursors. Journal of Physics D, Applied Physics, 2010, 43 (21): 215403–215411
23. Chino K, Koike J, Eguchi S, Araki H, Nakamura R, Jimbo K, Katagiri H. Preparation of Cu_2SnS_3 thin films by sulfurization of Cu/Sn stacked precursors. Japanese Journal of Applied Physics, 2012, 51(10): 10NC35-1–10NC35-4
24. Umehara M, Takeda Y, Motohiro T, Sakai T, Awano H, Maekawa R. $Cu_2Sn_{1-x}Ge_xS_3$ (x = 0.17) thin-film solar cells with high

conversion efficiency of 6.0%. Applied Physics Express, 2013, 6(4): 045501–045503

25. Naumkin A V, Kraut-Vass A, Gaarenstroom S W, Powell C J. NIST X-ray Photoelectron Spectroscopy Database, Version 4.1. 2013

Jun Han is currently a master student in Prof. Jiang Tang's group at Wuhan National Laboratory for Optoelectronics (WNLO) at Huazhong University of Science and Technology. She received her B.S. degree from Changchun University of Science and Technology in 2006. Her research focused on the hydrazine processed Cu_2SnS_3 thin film solar cell and its optoelectronic characteristics.

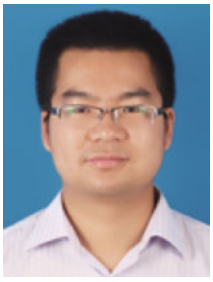

Jiang Tang is a Professor of Wuhan National Laboratory for Optoelectronics (WNLO) at Huazhong University of Science and Technology. He obtained his bachelor degree from University of Science and Technology of China, and his Ph.D degree from University of Toronto under the supervision of Prof. Edward H. Sargent. He then did his postdoctoral research at IBM T. J. Watson Research Center working on copper zinc tin sulfide solar cells. He was honored "National 1000 Young Talents" in 2012 and won "National Natural Science Fund for Excellent Young Scholar" in 2013. He has published over 20 papers on solar cells with 3 being cited over 100 times. His current research focuses on thin film photovoltaics using earth-abudant and nontoxic materials.